Geophysical Research Letters

RESEARCH LETTER
10.1029/2023GL106283

Detection and Attribution of Human-Perceived Warming Over China

Jintao Zhang[1,2,3], **Guoyu Ren**[2,4], **and Qinglong You**[3,5]

[1]Chinese Academy of Meteorological Sciences, China Meteorological Administration, Beijing, China, [2]National Climate Center, China Meteorological Administration, Beijing, China, [3]Department of Atmospheric and Oceanic Sciences, Fudan University, Shanghai, China, [4]Department of Atmospheric Science, School of Environmental Studies, China University of Geosciences, Wuhan, China, [5]CMA-FDU Joint Laboratory of Marine Meteorology, Shanghai, China

Key Points:

- The warming is quantified by human-perceived temperature that considers the joint effects of temperature, humidity and/or wind speed
- Human influence could be robustly detected in both summer and winter human-perceived warming
- The observed increase in human-perceived temperature is mostly attributed to anthropogenic greenhouse gas increases

Supporting Information:

Supporting Information may be found in the online version of this article.

Correspondence to:

G. Ren,
guoyoo@cma.gov.cn

Citation:

Zhang, J., Ren, G., & You, Q. (2024). Detection and attribution of human-perceived warming over China. *Geophysical Research Letters*, *51*, e2023GL106283. https://doi.org/10.1029/2023GL106283

Received 7 SEP 2023
Accepted 21 FEB 2024

Author Contributions:

Conceptualization: Jintao Zhang
Methodology: Jintao Zhang, Guoyu Ren
Writing – original draft: Jintao Zhang
Writing – review & editing: Guoyu Ren, Qinglong You

Abstract While previous studies have largely focused on anthropogenic warming characterized by surface air temperature, little is known about the behaviors of human-perceived temperature (HPT), which describe the "feels-like" equivalent temperature by considering the joint effects of temperature, humidity and/or wind speed. Here we adopted an optimal fingerprinting method to compare seasonal mean HPTs in China with those from simulations conducted with multiple climate models participating in the Coupled Model Intercomparison Project Phase 6. We found clear anthropogenic signals in the observational records of changes in both summer and winter HPTs over the period 1971–2020. Moreover, the anthropogenic greenhouse gas influence was robustly detected, with clear separation from natural and anthropogenic aerosol forcings. The anthropogenic greenhouse gas forcing plays the dominant role (>90%) of human-perceived warming. Urbanization effects contribute slightly and moderately to the estimated trends in summer and winter HPTs, respectively, in addition to the effects of external forcing.

Plain Language Summary Human influences have been identified in the observed warming quantified by surface air temperature (SAT), but SAT alone is inadequate as a metric for human thermal comfort. Here we focus on human-perceived temperature (HPT), which describes the "feels-like" equivalent temperature by considering the joint effects of temperature, humidity, and/or wind speed. We isolate anthropogenic impacts on the observed increase in summer and winter HPTs in China during 1971–2020 by comparing observations with state-of-the-art climate models. Results show that the influence of anthropogenic greenhouse gas is detected, with clear separation from other external forcings such as solar and volcanic activities and anthropogenic aerosols. The human-induced greenhouse gas increases are also found to explain most (>90%) of the observed human-perceived warming. Along with the effects of large-scale anthropogenic forcing, urbanization effects also have a slight to moderate influence on the estimated trends in summer and winter HPTs. Our work is an early attempt to provide quantitative evidence for the physiological impacts of anthropogenic global warming and local urbanization on human beings.

1. Introduction

Due to the rapid global warming that has occurred over the past century and its profound impacts on human society, climate change has come under more and more scrutiny from governments, the public, and the media. According to the Sixth Assessment Report of the Intergovernmental Panel on Climate Change (IPCC), the global mean near-surface temperature in 2011–2020 was 1.09 [0.95 to 1.20] °C higher than the preindustrial level (IPCC, 2021). As global mean temperature rises, the warm temperature extremes have increased and the cold extremes have decreased since the mid-20th century in most global land regions (Alexander et al., 2006; Dunn et al., 2020; P. Zhang et al., 2019; H. Zhang et al., 2023).

Although the global warming revealed by temperature-based observations are large and significant, they may not always be consistent with how people feel because the human body's thermal sensations are determined by the combined influence of meteorological factors such as temperature, humidity, wind speed, and solar radiation (de Freitas & Grigorieva, 2015; F. Wang et al., 2022). In hot summers, high humidity prevents perspiration from the skin to the environment, aggravating heat stress for people (Lin et al., 2019; J. Zhang et al., 2023). By contrast, high wind speed during cold winters can swiftly reduce the body's ability to store heat and significantly aggravate how chilly people feel. Human-perceived temperature (HPT) describes the "feels-like" equivalent temperature by considering the joint effects of the aforementioned meteorological factors (J. Li et al., 2018; Y. Wang et al., 2019).

Evidence has shown that extreme HPTs, including heat stress and wind chill, could reduce labor productivity and lead to illnesses and even fatalities (Dunne et al., 2013; Patz et al., 2005). Meanwhile, the usage of natural resources (e.g., fossil fuels for heating and air conditioning) and ensuing economic expenditures are also increased to reduce human discomfort from extreme HPTs. Therefore, there is great value in studying HPT from a climatological perspective.

A better understanding of external drivers for these changes in thermal conditions represents an important basis for reliable future projection and sets an important scientific basis for climate change adaptation policy-making, in particular for a densely populated region such as eastern China. China has been rapidly warming since the 1960s at a rate that is almost twice as fast as the average change in the world. Estimates based on in situ observations indicate that the annual mean surface air temperature (SAT) increased by 1.44°C over the period 1961–2013, which can be attributable to greenhouse gases, other anthropogenic forcing (dominated by aerosols), and the impacts of urban heat islands (Y. Sun et al., 2016). Other studies have further confirmed the dominant role of anthropogenic forcings in temperature change (Xu et al., 2015; Yin & Sun, 2023). In addition, the signal of anthropogenic forcing can be detected in long-term changes in extreme temperatures in China (Hu & Sun, 2022; Lu et al., 2016; Yin et al., 2017). Anthropogenic forcing was proven to increase the probability of extreme summer heat in eastern China (Y. Sun et al., 2014). However, the aforementioned studies merely considered the role of temperature, which is not sufficiently representative of human-perceived warming. In response to this knowledge gap, several studies addressing long-term changes in HPTs in China have recently emerged (Luo & Lau, 2019; Ning et al., 2022). In addition, there are also studies (J. Li et al., 2018; Wu et al., 2017; J.-T. Zhang et al., 2022) suggesting that China has experienced an increase in warm-uncomfortable days and a decrease in cold-uncomfortable days over the past decades from the perspective of HPT. However, the aforementioned studies did not fully address what caused the change. Although recent studies reported that human influences have increased the probability of summer compound heat-humidity extremes (Kong et al., 2020; C. Li et al., 2020; D.-Q. Wang & Sun, 2022), it cannot be assumed that those results are directly and comprehensively indicative of potential human influences on HPT (both heat stress and wind chill) in China. Moreover, to the best of our knowledge, similar detection and attribution studies have not been conducted in other regions.

This study aims to investigate the possible human influence on HPTs in China and pay particular attention to the possibility of separating the influence of anthropogenic greenhouse gases from other forcings such as aerosols, as the availability of simulations from the Detection and Attribution Model Intercomparison Project (DAMIP; Gillett et al., 2016) component of the Coupled Model Intercomparison Project Phase 6 (CMIP6; Eyring et al., 2016) offers a unique opportunity to do so. By comparing the evolution of HPT in the observations and model simulations under different external forcings, we investigate whether the anthropogenic influence is detectable in the historical seasonal mean HPT changes. This is done using statistically rigorous "fingerprint" analysis.

The paper is organized as follows. Section 2 describes observational and model data used in this study, along with an introduction to the data processing and attribution analysis method. We then present the results in Section 3 and conclude the study in Section 4.

2. Data and Methods

2.1. Human-Perceived Temperatures

Following previous studies (Ding et al., 2021; Y. Wang et al., 2019; J. Zhang et al., 2023), we adopted the wet bulb globe temperature (WBGT) and the wind chill temperature (WCT) to measure heat and cold perceived temperatures, respectively; accordingly, WBGT (WCT) was calculated for the summer (winter) months.

Specifically, the WBGT (°C) is calculated as a weighted value of daily mean SAT (T, °C) and wet bulb temperature (WBT, °C), as $\mathrm{WBGT} = 0.3\mathrm{T} + 0.7\mathrm{WBT}$, where WBT is calculated based on daily mean SAT and relative humidity using the estimator of Stull (2011). Other more sophisticated WBGT estimates require additional variables such as wind speed, solar radiation, and surface air pressure (e.g., Davies-Jones, 2008; Lemke & Kjellstrom, 2012; Liljegren et al., 2008), while reliable observations and simulations for some of these variables are limited. Although we acknowledged that WBT is adopted to measure human heat stress in some climate change studies (e.g., Pal & Eltahir, 2016; Raymond et al., 2017; P. Wang et al., 2021), WBT is not well calibrated as a heat stress metric and no safety thresholds are recognized by the medical community (Schwingshackl

et al., 2021; Sherwood, 2018; J. Zhang et al., 2023). Therefore, we employed WBGT instead of WBT in this study.

When $-50°C \le T \le 10°C$, the WCT can be calculated from daily mean SAT (T, °C) and wind speed (V, m s^{-1}) as follows (Ding et al., 2021; Osczevski & Bluestein, 2005)

$$\mathrm{WCT} = \begin{cases} 13.12 + 0.6215T - 13.9563V^{0.16} + 0.4867TV^{0.16}, V \ge 1.389 \\ T - 1.1448V + 0.0968TV, V < 1.389 \end{cases} \quad (1)$$

When $T > 10°C$, the WCT is defined by the universal apparent temperature calculated from T, V, and water vapor pressure (P, kPa) from Steadman (1984).

$$\mathrm{WCT} = -2.7 + 1.04T + 2P - 0.65V \quad (2)$$

2.2. Observations

We used daily mean SAT, relative humidity, and wind speed observations from 2,419 national meteorological stations in China's mainland, which have been strictly quality-controlled, including checks for climatological, station, and regional outliers, and for internal, temporal, and spatial consistency (Ren et al., 2012). Temperature and relative humidity data have been further homogenized (Cao et al., 2016; Zhu et al., 2015). Given that data before 1970 contains a significant number of missing values and that the observational instrumentation underwent a significant change in the late 1960s (X. Li et al., 2022; Yang et al., 2021), the study period was defined as 1971–2020. Note that the 1971 winter consists of data averaged from November 1970 through March 1971, the 1972 winter consists of data averaged from November 1971 through March 1972, and so on. Daily HPTs can be calculated on this basis.

We used the following criteria to select stations for the subsequent analysis: (a) the percentage of missing data throughout the study period is no more than 0.2%, and (b) the percentage of missing data for any of these years is no more than 5%. As a result, a total of 2112 (1638) stations were selected for investigating summer (winter) HPTs, and their distribution is shown in Figure S1 in Supporting Information S1. The missing records were replaced by the climatological mean value of the same calendar day for the given station.

For each station, we calculated the mean WBGT for extended summer (May–September) and the mean WCT for extended winter (November–March) by averaging daily values over the five months. Summer WBGT (winter WCT) anomalies relative to a 1971–2000 baseline period were then computed. The resulting station anomalies are aggregated to $5° \times 5°$ grid cell anomalies by averaging all available station anomalies within a predefined grid cell (Figure S1 in Supporting Information S1). The regional-averaged anomalies were obtained by area-weighted averaging of the values of all the grids, with the weights assigned as the cosine midlatitude values of the grids (Ren & Zhou, 2014).

2.3. Model Data

Daily mean SAT, relative humidity, and wind speed outputs from global climate models participating in CMIP6 were adopted in this study. First, we used the historical (ALL) simulations for 1971–2014, where climate models are forced with both anthropogenic (greenhouse gas and aerosol) and natural (solar and volcanic) external forcings. Each ALL simulation has been extended until 2020 by using the SSP2-4.5 scenario simulation (O'Neill et al., 2016). To explore the influence of individual external forcings, we also utilized historical individual forcing simulations for 1971–2020, including hist-GHG (GHG), hist-aer (AER), and hist-nat (NAT) experiments, where climate models are forced with only greenhouse gas, anthropogenic aerosol, and natural external forcing, respectively (Gillett et al., 2016). Simulations from eight CMIP6 models, which provide necessary data for all experiments of GHG, AER, and NAT with a minimum of three ensemble members, were used here (Table S1 in Supporting Information S1). Signals (i.e., model-simulated responses) are computed as multi-model ensemble mean (MME), which is done by first computing the arithmetical average for each model ensemble and then averaging the individual model means. In addition, we also used 386 nonoverlapping 50-year segments from unforced preindustrial control simulation (CTL) of 33 CMIP6 models to estimate natural climate variability

(Table S1 in Supporting Information S1). These 48-year segments, which are the same length as the observed record (1971–2020), are assigned calendar dates by designating the first year in each segment as 1971.

The model-simulated summer WBGT and winter WCT can be calculated similarly. All of the season mean HPTs were converted to anomalies relative to 1971–2000 and then remapped to the 5° × 5° grid. To ensure a fair comparison between observations and models, the remapped model data sets were masked according to the availability of observational data.

We acknowledged that detection and attribution assessments heavily rely on model simulations, thus it's critical to compare the results of model simulations to observations in order to increase confidence in the accuracy of the attribution results. It is shown that CMIP6 models adopted in this study reasonably reproduce the observed nonsecular interannual variability in seasonal mean HPTs, that is, the variability in the detrended seasonal mean HPTs (Figure S2 in Supporting Information S1). Similarity of the secular component of the seasonal mean HPT variability will be demonstrated in the subsequent detection and attribution analysis (Section 3).

2.4. Detection and Attribution

In this study, we employed the regularized optimal fingerprinting technique (Ribes et al., 2013) as a method for detection and attribution analysis to compare observed seasonal mean HPT changes to model simulations. This technique regresses the observations $\mathbf{Y}$ onto model-simulated signal patterns $\mathbf{X}$, plus internal climate variability $\boldsymbol{\varepsilon}$: $\mathbf{Y} = (\mathbf{X} - \nu)\boldsymbol{\beta} + \boldsymbol{\varepsilon}$, where ν represents the influence of natural internal variability in the modeled signal patterns. The regression coefficients $\boldsymbol{\beta}$ are unknown scaling factors that will be estimated via a total least square method (Allen & Stott, 2003). If the 90% confidence interval of $\boldsymbol{\beta}$ falls above zero, the corresponding modeled signals are considered to be detected in the observations. In these cases, if the 90% confidence interval of $\boldsymbol{\beta}$ also includes one, then the modeled responses are considered to be consistent with the observations (Allen & Stott, 2003; Ribes et al., 2013).

The observational vector, $\mathbf{Y}$, which describes the spacetime evolution of HPTs, is comprised of non-overlapping five-year-mean HPTs over two spatial dimensions representing eastern and western China. The 50-year record (1971–2020) generates 10 non-overlapping five-year averages. The east-west partitioning divides the country into two regions, with eastern China (EC; east of 105°E) having a typical monsoon climate and western China (WC; west of 105°E) having an arid or semiarid climate. This produces a 20-dimensional observational vector. Because of the distinct climates in the two regions, the division may offer a valuable contrast in signal patterns that can aid in identifying the effects of various forcing factors on observations using the optimal fingerprinting technique (Yin et al., 2017). We did not consider separate analysis for each region to reduce the risk of overfitting (C. Li et al., 2020; Y. Sun et al., 2016). Model data segments from forced and control simulations were also processed identically into 20-dimensional vectors.

Single-signal, two-signal, and three-signal analysis were performed in this study. For single-signal analysis, observed changes are regressed onto the forced response to historical ALL forcing. As the ALL forcing is a combination of anthropogenic forcing (ANT) and natural external forcing (NAT), we also conduct a two-signal analysis of the ANT (ANT = ALL − NAT) and NAT signals to further distinguish the individual role of ANT and NAT forcings in driving the observed changes. For three-signal analysis, responses to GHG forcing, AER forcing, and NAT forcing are involved simultaneously in the regression. A residual consistency test is applied to test whether the modeled internal variability is consistent with that observed as represented by regression residuals (Ribes et al., 2013).

We further estimated the changes attributable to the ALL forcing, and the GHG, AER, and NAT components of ALL forcing, by computing trends in the ALL, GHG, AER, and NAT signals and then multiplying them by the respective estimates of scaling factors (Hu & Sun, 2022). Note that such attributable changes were estimated based on the single- (for ALL) and three-signal analysis (for GHG, AER, and NAT). The linear trends in HPTs were estimated by the least square method, and the 5% level is used to define the statistically significant trend (Student's *t*-test). For model simulations, in addition to the trend for MME, we also calculated trends for individual models. If at least one significant individual trend differs in the sign of the ensemble mean trend, it is considered as "uncertain"; if the "uncertain" condition is not fulfilled and less than half of the individual trends are significant, it is considered as "negligible"; otherwise, the modeled signals are referred to as "robust" (J. Zhang et al., 2022).

In addition to the aforementioned external forcing factors, rapid urbanization in China in recent decades may have had a considerable effect on the estimated trends in HPTs, as urbanization alters the surface energy budget and results in higher temperatures in urban areas than in surrounding rural areas (Kong et al., 2020; Y. Sun et al., 2016; Y. Wang et al., 2019; Luo & Lau, 2021). To quantify this effect, following Tysa et al. (2019), the meteorological stations were classified into rural and urban stations, where the proportions of land use/land cover in different buffer areas around the stations were considered. The selection of rural station networks also referred to Ren et al. (2015), which considered the need to meet conditions of good continuity and integrity in the observational data, with more emphasis on the relocation of stations and the immunity of stations to the urbanization effect. For analysis of summer (winter) HPT, A total of 234 (192) stations were finally chosen as rural stations, while the remaining 1,878 (1,446) stations were considered urban stations (Figure S1 in Supporting Information S1). We first calculated the grid-averaged seasonal HPTs series of the national and rural stations for each grid, subsequently the regional-averaged HPTs series of the national and rural stations can be obtained. The urbanization effect (UE), which refers to the impact of urbanization on HPT trends, is defined as the difference between the national trend and the rural trend: $\Delta T_{u\text{-}r} = T_u\text{-}T_r$, and the relative urbanization contribution in percentage is given by $UC = |\Delta T_{u\text{-}r}/T_u| \times 100\%$ (Ren & Zhou, 2014).

Following Kong et al. (2020), we further adjusted the contributions of external forcings according to the contributions of urbanization:

$$\mathrm{coef}_{\mathrm{adj}} = \frac{C_{\mathrm{ALL}}}{\hat{C}_{\mathrm{ALL}}} = \frac{C_{\mathrm{whole}} \times (1 - \mathrm{UC})}{\hat{C}_{\mathrm{ALL}}} \tag{3}$$

$$\hat{C}_{x,\mathrm{adj}} = \hat{C}_x \times \mathrm{coef}_{\mathrm{adj}} \tag{4}$$

where $\hat{C}_x$ (x = ALL, GHG, AER, NAT) is the estimated changes attributable to external forcing (see the previous paragraph), C_{whole} is the observed change in HPTs over 1971–2020 (i.e., linear trend value multiplied by 50 years).

3. Results

3.1. Widespread Increases in HPTs in China During the Past Decades

Figure 1 shows trends in seasonal mean HPTs since 1971 in the observations and modeled responses to different forcings. Both summer and winter have significantly increased over all regions where there are sufficient data, with the most pronounced increases occurring in the northern part of China (Figures 1a and 1g). This trend pattern is also similar to that of seasonal mean SAT (Figures 2a and 2d), suggesting the dominant role of the rising air temperature in producing human-perceived warming. Seasonally, the upward trend in the country-averaged summer HPT (0.27°C/decade) resembles that in summer air temperature (0.29°C/decade), which can be explained by the fact that relative humidity exhibits little trend in almost all regions (Figure 2c). In contrast, the increasing trend in the country-averaged winter HPT (0.54°C/decade) is considerably greater than that in winter mean SAT (0.38°C/decade), suggesting the role of other meteorological factors. It is shown that the winter mean near-surface wind speeds have declined significantly in the majority of China, and while this trend has been reversed in some regions in the last decade or two (Ding et al., 2021; X. Li et al., 2022), the overall trend since 1971 is still declining (Figure 2f). The combination of rising temperatures and weakening winds leads to rapid human-perceived winter warming over China. In addition, we also recognize a slowdown of warming in winter HPT after the late 1990s (Figure 3b), which is in line with previous studies (X. Sun et al., 2017; Ding et al., 2021; J.-T. Zhang et al., 2022). Both the insignificant trend of mean temperature and the increasing trend of the wind speed contribute to the slowdown of the human-perceived winter warming after the late 1990s, and this conjoint contribution could be linked to the decadal variability of East Asian winter monsoon circulations (Ding et al., 2021).

Widespread increases in seasonal mean HPTs are also found in simulations when anthropogenic emissions of greenhouse gases are included as external forcing. The spatial pattern of the trends in ALL responses roughly resembles that observed (Figures 1c and 1i). The observed trends lie within the range of trends in the ensemble of multi-model simulations in all grid cells except some isolated outliers where the observations show weaker (stronger) warming trends in summer (winter) HPTs (Figure S3 in Supporting Information S1). The GHG

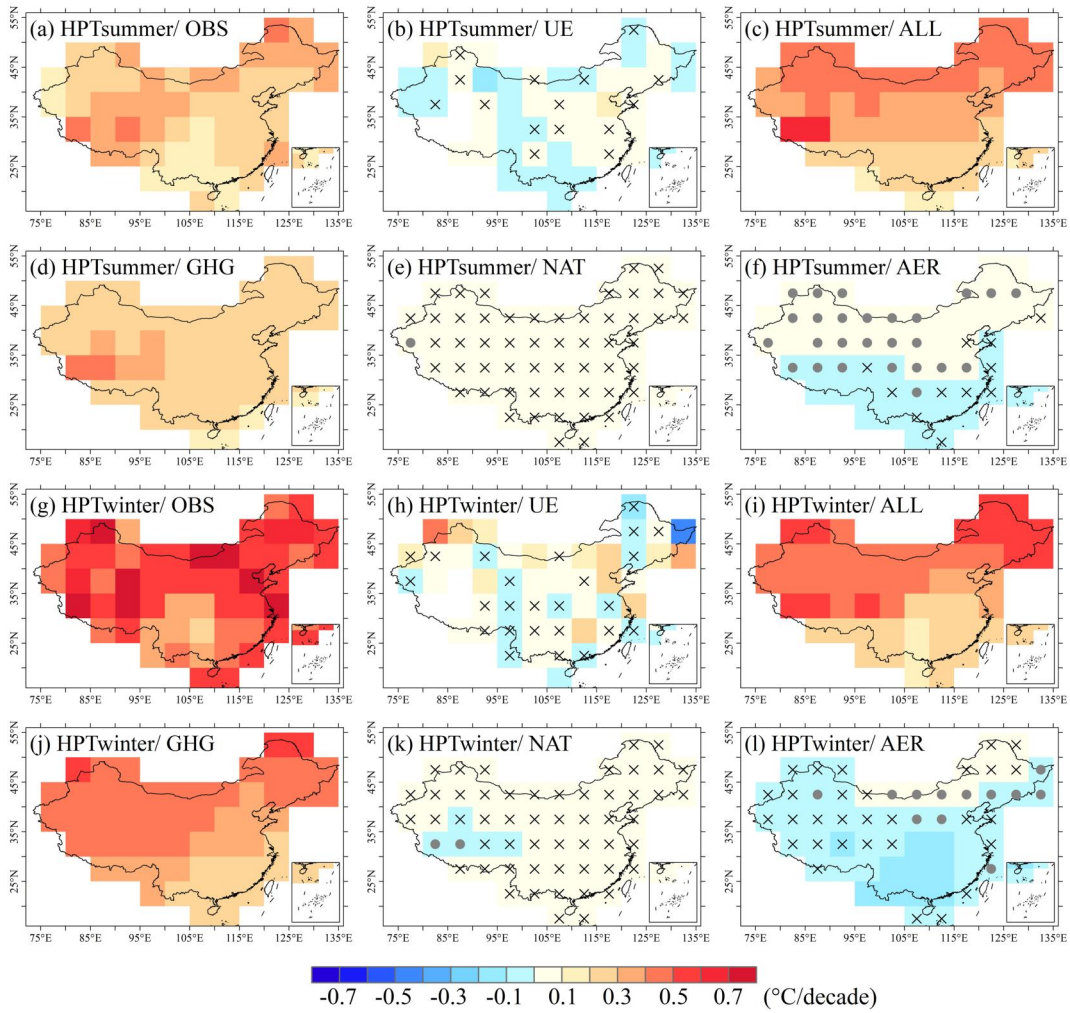

Figure 1. Spatial distribution of linear trends in seasonal mean HPTs during 1971–2020 from observations (OBS), the urbanization effect (UE), and CMIP6 multi-model simulations forced with all forcing (ALL), only greenhouse gas (GHG), anthropogenic aerosol (AER), and natural forcing (NAT). (a)–(f): Summer mean HPT. (g)–(l): Winter mean HPT. The crosses in observational results, that is, OBS and UE, indicate the trends are NOT statistically significant ($p > 0.05$). The crosses and dots in model-simulated results, that is, ALL, GHG, NAT, and AER, indicate negligible and uncertain trends, respectively.

responses have a trend spatial pattern similar to the ALL responses (Figures 1d and 1j), and capture the majority of the observed trends as well (Figure S3 in Supporting Information S1). By contrast, trends in the NAT responses are very small and negligible (Figures 1e and 1k), and the observed trends lie above the 95th percentile of trends computed from individual NAT runs in all grid cells (Figure S3 in Supporting Information S1). In addition, the AER response exhibits an overall weak cooling pattern, despite the uncertainties in the results of the individual models (Figures 1f and 1l). The observed time series of country-averaged seasonal mean HPTs is generally within the range of simulations under ALL forcing, but it is all above the range of simulations under NAT forcing. All modeled responses to ALL and GHG show positive trends. Trends in the modeled responses to NAT forcing are very weak. The AER responses show a weak negative trend for winter HPT (Figures 3a and 3b).

Considering that the in situ observation data have a systematic bias caused by urbanization around the observational sites in many regions over the past decades (Ren & Zhou, 2014; P. Zhang et al., 2021), we further evaluate the urbanization effect on estimates of trends in season mean HPTs based on differences in national and rural trends. The urbanization effect for China as a whole is 0.02 and 0.27°C per 50 yr, for summer and winter HPTs, respectively, all statistically significant at the 5% significance level, with urbanization

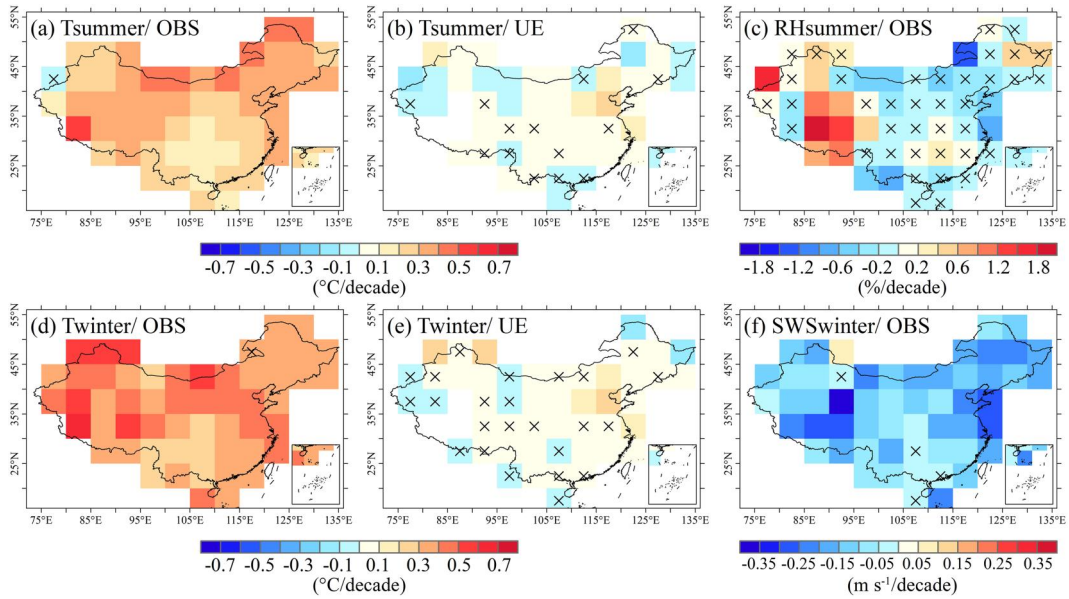

Figure 2. Spatial distribution of observed linear trends in seasonal mean temperature and other relevant meteorological variables during 1971–2020. (a)–(b): Summer mean near-surface air temperature. (c): Summer mean near-surface relative humidity (RH). (d)–(e): Winter mean near-surface air temperature. (f): Winter mean near-surface wind speed (SWS). The crosses indicate the trends are NOT statistically significant ($p > 0.05$).

contributions being 1.8% and 10.4%, respectively. More grids register significant positive urbanization effects for winter HPT than for summer HPT (Figures 1b and 1h). Correspondingly, the urbanization contribution to summer and winter mean SAT is 8.2% and 9.5%, respectively (Figures 2b and 2e). The lower urbanization contribution to summer HPT lines up with earlier research that found the urban dry island effect (Huang et al., 2022; P. Wang et al., 2022) partially negates the impact of higher air temperatures and consequently moderates urban heat stress, which is characterized by HPTs (Chakraborty et al., 2022; X. Wang & Gong, 2010). By contrast, it is anticipated that the urbanization-induced decline in surface wind speed (Z. Li et al., 2018; Lin et al., 2019) will widen the gap in the winter wind chill temperature between rural and urban areas, and further increase the winter mean HPT at the urban stations.

3.2. The Increase in HPTs Is Driven Primarily by Human Influence on the Climate

In this section, we report results from fingerprinting analysis confirming statistical evidence for the role of human influence in the observed long-term HPT increase. For single-signal analysis, the estimates of the scaling factors for both summer and winter HPTs are greater than zero, indicating that the ALL signals are robustly detected at the 5% significance level (Figures 3c and 3d). Seasonally, the best estimate of the scaling factor for summer (winter) HPT is marginally smaller (greater) than one, indicating that available CMIP6 models slightly overestimate (underestimate) the rate of the human-perceived warming in summer (winter). This bias in the model-simulated results also presents in the upward evolution of seasonal mean air temperatures over the same period (Figure S4 in Supporting Information S1). Estimates of the ANT and NAT scaling factors from two-signal analysis suggest that the ANT signals can be detected, while the NAT signals cannot be detected, for both summer and winter HPTs (Figures 3c and 3d). For summer (winter) HPT, the 90% confidence interval of the scaling factor is approximately one (exceeded one), indicating that the ANT responses from analyzed CMIP6 models are consistent with observations (tend to slightly underestimate the observed changes). The detectability of ALL and ANT forcings does not appear to have been affected, although a slowdown of warming in winter HPT after the late 1990s is evident. This study is the first one to provide direct evidence for the dominant anthropogenic role in the observed human-perceived warming in China, despite similar analysis for summer/winter mean SAT suggests that anthropogenic influence is dominant, while natural influence is not detectable, at the same significance level (Figure S4 in Supporting Information S1).

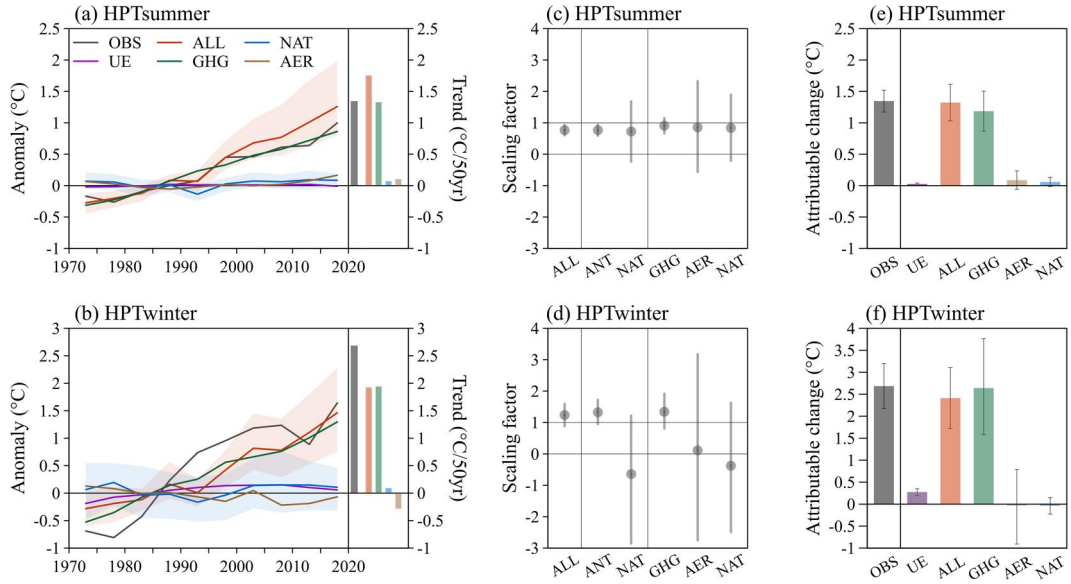

Figure 3. Results of detection and attribution analysis for seasonal mean HPTs. (Left column; a–b) Time series of five-year mean anomaly values (relative to 1971–2000) for country-averaged summer and winter HPTs, based on the observations (OBS; black) and the CMIP6 multi-model response to the ALL (red), GHG (green), AER (brown), and NAT (blue) forcings. The red and blue shadings in the time series show the 5%–95% range of the ALL and NAT simulations, respectively. The urbanization effect (UE), expressed as the differences between the urban and rural stations, is shown in purple curves. The corresponding linear trends are shown in the immediate right panel. (Middle column; c–d) Best estimates of scaling factors and their 5–95% confidence intervals from single-signal analysis for ALL forcing, two-signal analysis for ANT and NAT forcings, and three-signal analysis for GHG, AER, and NAT forcings in summer and winter HPTs for the period 1971–2020. (Right column; e–f) Attributable contribution from ALL, GHG, AER, and NAT forcings, as well as UE, to observational trend (OBS) in summer and winter HPTs for the period 1971–2020, and their 5–95% confidence interval (error bars).

Furthermore, for three-signal analysis, only the GHG signal can be detected when the signals of GHG, AER, and NAT are considered simultaneously. This result holds for both summer and winter HPTs (Figures 3c and 3d). Similar to the ANT forcing results, the best estimates of scaling factors for GHG forcing were greater than one for winter HPT and close to one for summer HPT. We also performed the same three-signal analysis for SAT as for HPT (Figure S4 in Supporting Information S1). While showing the similar detectability, it cannot be assumed that those results are directly and comprehensively representative of the human-perceived warming. The AER signals are not detectable in this study, either for HPT or for SAT (Figure 3 and Figure S4 in Supporting Information S1), despite prior studies reporting that they can be detected for observed temperature changes in China since the 1950s in some cases (Hu & Sun, 2022; Yin & Sun, 2023). This suggests low detectability of the AER signal within a short period against natural variability. The low AER signal detectability is probably due to the shorter period analyzed in this paper than those in previous works, and the alleviation of air pollution over the last two decades (Sogacheva et al., 2018). It may also have been related to the strong collinearity between the GHG and AER results (DelSole et al., 2019; Jones et al., 2013).

It is noticed that the confidence intervals of the scaling factors for summer HPT are generally narrower than those for winter HPT, suggesting that human influence is more detectable in summer warming, which is in line with previous SAT-based studies (Yin & Sun, 2023; Zhou & Zhang, 2021). Moreover, the residual consistency test passed for all the above cases, indicating a good agreement between model-simulated variability and observations (Allen & Stott, 2003).

We further estimate the human-perceived warming attributable to the urbanization effect, ALL forcing, and the GHG, AER, and NAT components of ALL forcing (Figures 3e and 3f). The observed country-averaged summer and winter HPTs increased by approximately 1.35°C (90% confidence interval 1.17–1.52°C) and 2.69°C (2.17–3.20°C), in which the ALL contributed to 1.32°C (1.03–1.61°C) and 2.41°C (1.72–3.11°C) of warming, respectively. The warming rate of HPTs is higher at urban stations than in rural stations, and quantitative attribution analysis shows that urbanization contributes to 1.8% and 10.4% of the human-

perceived summer and winter warming over China since the early 1970s, respectively. The GHG contributed to 1.19°C (0.87–1.50°C) and 2.64°C (1.58–3.76°C) of warming for summer and winter HPTs, respectively. The contributions of AER and NAT are not considered for both summer and winter HPTs, as their confidence intervals included zero. The above results suggest that the GHG forcing is the dominant contributor (>90%) to human-perceived warming in both summer and winter. Although the AER forcing seems to exhibit a cooling effect for winter HPT, it is not detectable at the 5% significance level. The NAT forcing effects are negligible in all cases. As a sensitivity test, we also performed separate analysis for each region (i.e., WC and EC), despite the potential for increasing the risk of overfitting. The results show that human contributions at the regional scale are also similar to those at the national scale (Figure S5 in Supporting Information S1).

4. Conclusion and Discussions

Although there is already overwhelming evidence that human influence has warmed the atmosphere beyond a reasonable doubt (IPCC, 2021), it remains unclear to what extent external drivers contribute to "sensible" climate change as perceived by the human body. Based on in situ observations and CMIP6-DAMIP simulations, this study investigates human-perceived summer and winter warming over China. Clear evidence of warming is observed in summer and winter HPTs, with magnitudes of 1.35 and 2.69°C over the period 1971–2020, respectively. The CMIP6 models reasonably reproduce the aforementioned warming features, demonstrating usually good agreement with observations in summer HPT but slightly overestimating observed changes in winter HPT. The reasons behind these changes are further investigated from a viewpoint of external forcing by applying an optimal fingerprinting method. Both the ALL and ANT signals can be detected in both summer and winter HPTs. Moreover, the three-signal detections suggest that the GHG signal can be clearly detected whereas the AER signal is less detectable. The NAT forcing effects are negligible in all cases. Changes separately attributable to different factors confirm the dominant role of the GHG forcing in human-perceived warming. Urbanization effects also have a slight to moderate influence on the estimated trends in summer and winter HPTs, respectively, in addition to the effects of large-scale anthropogenic forcing. Our study can provide a better understanding of the physiological impacts of anthropogenic global warming and local urbanization on human beings and is crucial for adapting to climate change at the regional scale.

Although HPTs have likely changed significantly for all seasons, here we concentrate on the hottest (summer) and coldest (winter) situations, which are also the ones with the greatest impacts on human health. We also acknowledged that more complex HPTs based on the human heat exchange model, such as Physiological Equivalent Temperature (PET; Höppe, 1999) and Universal Thermal Climate Index (UTCI; Bröde et al., 2012), are expected to give more accurate results, these HPTs, however, cannot be calculated from the standard meteorological variables in observations and model outputs. Moreover, considering that there are increasingly fewer stations in China that are completely free of urban influences, and the lowered standard for determining the rural stations (Tysa et al., 2019), the urbanization effects and contributions estimated by the differences in urban and rural HPT trends are likely to be conservative (Ren & Zhou, 2014; Y. Sun et al., 2016).

Data Availability Statement

Outputs from CMIP6 models (Eyring et al., 2023) were used in the creation of this manuscript, which are available at the Lawrence Livermore National Laboratory website (https://esgf-node.llnl.gov/search/cmip6/). The China Meteorological Data Service Center provides the daily observations. Because we are not authorized to share original observed data, we archived all the processed data including observed and simulated HPTs on Zenodo (Zhang et al., 2023), which is available at https://doi.org/10.5281/zenodo.10223710.

Acknowledgments
This study is supported by the National Key Research and Development Program of China (2018YFA0605603). We sincerely thank the reviewers for their excellent comments and suggestions. We thank the China Meteorological Administration for providing the observational data. We also thank the climate modeling groups for producing and making available their model output.

References

Alexander, L. V., Zhang, X., Peterson, T. C., Caesar, J., Gleason, B., Klein Tank, A. M. G., et al. (2006). Global observed changes in daily climate extremes of temperature and precipitation. *Journal of Geophysical Research*, *111*(D5), D05109. https://doi.org/10.1029/2005JD006290

Allen, M. R., & Stott, P. A. (2003). Estimating signal amplitudes in optimal fingerprinting, part I: Theory. *Climate Dynamics*, *21*(5–6), 477–491. https://doi.org/10.1007/s00382-003-0313-9

Bröde, P., Fiala, D., Błażejczyk, K., Holmér, I., Jendritzky, G., Kampmann, B., et al. (2012). Deriving the operational procedure for the universal thermal climate index (UTCI). *International Journal of Biometeorology*, *56*(3), 481–494. https://doi.org/10.1007/s00484-011-0454-1

Cao, L., Zhu, Y., Tang, G., Yuan, F., & Yan, Z. (2016). Climatic warming in China according to a homogenized data set from 2419 stations. *International Journal of Climatology*, *36*(13), 4384–4392. https://doi.org/10.1002/joc.4639

Chakraborty, T., Venter, Z. S., Qian, Y., & Lee, X. (2022). Lower urban humidity moderates outdoor heat stress. *AGU Advances*, *3*(5). https://doi.org/10.1029/2022AV000729

Davies-Jones, R. (2008). An efficient and accurate method for computing the wet-bulb temperature along pseudoadiabats. *Monthly Weather Review*, *136*(7), 2764–2785. https://doi.org/10.1175/2007MWR2224.1

de Freitas, C. R., & Grigorieva, E. A. (2015). A comprehensive catalogue and classification of human thermal climate indices. *International Journal of Biometeorology*, *59*(1), 109–120. https://doi.org/10.1007/s00484-014-0819-3

DelSole, T., Trenary, L., Yan, X., & Tippett, M. K. (2019). Confidence intervals in optimal fingerprinting. *Climate Dynamics*, *52*(7–8), 4111–4126. https://doi.org/10.1007/s00382-018-4356-3

Ding, T., Gao, H., & Li, X. (2021). Universal pause of the human-perceived winter warming in the 21st century over China. *Environmental Research Letters*, *16*(6), 064070. https://doi.org/10.1088/1748-9326/ac037a

Dunn, R. J. H., Alexander, L. V., Donat, M. G., Zhang, X., Bador, M., Herold, N., et al. (2020). Development of an updated global land in situ-based data set of temperature and precipitation extremes: HadEX3. *Journal of Geophysical Research: Atmospheres*, *125*(16), e2019JD032263. https://doi.org/10.1029/2019JD032263

Dunne, J. P., Stouffer, R. J., & John, J. G. (2013). Reductions in labour capacity from heat stress under climate warming. *Nature Climate Change*, *3*(6), 563–566. https://doi.org/10.1038/nclimate1827

Eyring, V., Bony, S., Meehl, G. A., Senior, C. A., Stevens, B., Stouffer, R. J., & Taylor, K. E. (2016). Overview of the Coupled Model Intercomparison Project Phase 6 (CMIP6) experimental design and organization. *Geoscientific Model Development*, *9*(5), 1937–1958. https://doi.org/10.5194/gmd-9-1937-2016

Eyring, V., Bony, S., Meehl, G. A., Senior, C. A., Stevens, B., Stouffer, R. J., & Taylor, K. E. (2023). Model output prepared for CMIP6 [Dataset]. Earth System Grid Federation. https://esgf-node.llnl.gov/search/cmip6/

Gillett, N. P., Shiogama, H., Funke, B., Hegerl, G., Knutti, R., Matthes, K., et al. (2016). The detection and attribution model intercomparison project (DAMIP v1.0) contribution to CMIP6. *Geoscientific Model Development*, *9*(10), 3685–3697. https://doi.org/10.5194/gmd-9-3685-2016

Höppe, P. (1999). The physiological equivalent temperature - A universal index for the biometeorological assessment of the thermal environment. *International Journal of Biometeorology*, *43*(2), 71–75. https://doi.org/10.1007/s004840050118

Hu, T., & Sun, Y. (2022). Anthropogenic influence on extreme temperatures in China based on CMIP6 models. *International Journal of Climatology*, *42*(5), 2981–2995. https://doi.org/10.1002/joc.7402

Huang, X., Hao, L., Sun, G., Yang, Z., Li, W., & Chen, D. (2022). Urbanization aggravates effects of global warming on local atmospheric drying. *Geophysical Research Letters*, *49*(2), e2021GL095709. https://doi.org/10.1029/2021GL095709

IPCC. (2021). Summary for policymakers. In V. Masson-Delmotte, P. Zhai, A. Pirani, S. L. Connors, C. Péan, et al. (Eds.), *Climate change 2021: The physical science basis. Contribution of working group I to the sixth assessment report of the intergovernmental panel on climate change* (pp. 3–32). Cambridge University Press. https://doi.org/10.1017/9781009157896.001

Jones, G. S., Stott, P. A., & Christidis, N. (2013). Attribution of observed historical near-surface temperature variations to anthropogenic and natural causes using CMIP5 simulations. *Journal of Geophysical Research: Atmospheres*, *118*(10), 4001–4024. https://doi.org/10.1002/jgrd.50239

Kong, D., Gu, X., Li, J., Ren, G., & Liu, J. (2020). Contributions of global warming and urbanization to the intensification of human-perceived heatwaves over China. *Journal of Geophysical Research: Atmospheres*, *125*(18), e2019JD032175. https://doi.org/10.1029/2019JD032175

Lemke, B., & Kjellstrom, T. (2012). Calculating workplace WBGT from meteorological data: A tool for climate change assessment. *Industrial Health*, *50*(4), 267–278. https://doi.org/10.2486/indhealth.MS1352

Li, C., Sun, Y., Zwiers, F., Wang, D., Zhang, X., Chen, G., & Wu, H. (2020). Rapid warming in summer wet bulb globe temperature in China with human-induced climate change. *Journal of Climate*, *33*(13), 5697–5711. https://doi.org/10.1175/JCLI-D-19-0492.1

Li, J., Chen, Y. D., Gan, T. Y., & Lau, N.-C. (2018). Elevated increases in human-perceived temperature under climate warming. *Nature Climate Change*, *8*(1), 43–47. https://doi.org/10.1038/s41558-017-0036-2

Li, X., Li, Q.-P., Ding, Y.-H., & Wang, M. (2022). Near-surface wind speed changes in eastern China during 1970–2019 winter and its possible causes. *Advances in Climate Change Research*, *13*(2), 228–239. https://doi.org/10.1016/j.accre.2022.01.003

Li, Z., Song, L., Ma, H., Xiao, J., Wang, K., & Chen, L. (2018). Observed surface wind speed declining induced by urbanization in East China. *Climate Dynamics*, *50*(3–4), 735–749. https://doi.org/10.1007/s00382-017-3637-6

Liljegren, J. C., Carhart, R. A., Lawday, P., Tschopp, S., & Sharp, R. (2008). Modeling the wet bulb globe temperature using standard meteorological measurements. *Journal of Occupational and Environmental Hygiene*, *5*(10), 645–655. https://doi.org/10.1080/15459620802310770

Lin, L., Luo, M., Chan, T. O., Ge, E., Liu, X., Zhao, Y., & Liao, W. (2019). Effects of urbanization on winter wind chill conditions over China. *Science of the Total Environment*, *688*, 389–397. https://doi.org/10.1016/j.scitotenv.2019.06.145

Lu, C., Sun, Y., Wan, H., Zhang, X., & Yin, H. (2016). Anthropogenic influence on the frequency of extreme temperatures in China. *Geophysical Research Letters*, *43*(12), 6511–6518. https://doi.org/10.1002/2016GL069296

Luo, M., & Lau, N. (2021). Increasing human-perceived heat stress risks exacerbated by urbanization in China: A comparative study based on multiple metrics. *Earth's Future*, *9*(7), e2020EF001848. https://doi.org/10.1029/2020EF001848

Luo, M., & Lau, N.-C. (2019). Characteristics of summer heat stress in China during 1979–2014: Climatology and long-term trends. *Climate Dynamics*, *53*(9), 5375–5388. https://doi.org/10.1007/s00382-019-04871-5

Ning, G., Luo, M., Wang, S., Liu, Z., Wang, P., & Yang, Y. (2022). Dominant modes of summer wet bulb temperature in China. *Climate Dynamics*, *59*(5–6), 1473–1488. https://doi.org/10.1007/s00382-021-06051-w

O'Neill, B. C., Tebaldi, C., van Vuuren, D. P., Eyring, V., Friedlingstein, P., Hurtt, G., et al. (2016). The scenario model intercomparison project (ScenarioMIP) for CMIP6. *Geoscientific Model Development*, *9*(9), 3461–3482. https://doi.org/10.5194/gmd-9-3461-2016

Osczevski, R., & Bluestein, M. (2005). The new wind chill equivalent temperature chart. *Bulletin of the American Meteorological Society*, *86*(10), 1453–1458. https://doi.org/10.1175/BAMS-86-10-1453

Pal, J. S., & Eltahir, E. A. B. (2016). Future temperature in southwest Asia projected to exceed a threshold for human adaptability. *Nature Climate Change*, *6*(2), 197–200. https://doi.org/10.1038/nclimate2833

Patz, J. A., Campbell-Lendrum, D., Holloway, T., & Foley, J. A. (2005). Impact of regional climate change on human health. *Nature*, *438*(7066), 310–317. https://doi.org/10.1038/nature04188

Raymond, C., Singh, D., & Horton, R. M. (2017). Spatiotemporal patterns and synoptics of extreme wet-bulb temperature in the contiguous United States. *Journal of Geophysical Research: Atmospheres*, *122*(24), 13108–13124. https://doi.org/10.1002/2017JD027140

Ren, G., Li, J., Ren, Y., Chu, Z., Zhang, A., Zhou, Y., et al. (2015). An integrated procedure to determine a reference station network for evaluating and adjusting urban bias in surface air temperature data. *Journal of Applied Meteorology and Climatology*, *54*(6), 1248–1266. https://doi.org/10.1175/JAMC-D-14-0295.1

Ren, G., & Zhou, Y. (2014). Urbanization effect on trends of extreme temperature indices of national stations over mainland China, 1961–2008. *Journal of Climate*, *27*(6), 2340–2360. https://doi.org/10.1175/JCLI-D-13-00393.1

Ren, Z., Yu, Y., Zou, F., & Xu, Y. (2012). Quality detection of surface historical basic meteorological data (in Chinese). *Journal of Applied Meteorological Science*, *23*(6), 739–747.

Ribes, A., Planton, S., & Terray, L. (2013). Application of regularised optimal fingerprinting to attribution. Part I: Method, properties and idealised analysis. *Climate Dynamics*, *41*(11–12), 2817–2836. https://doi.org/10.1007/s00382-013-1735-7

Schwingshackl, C., Sillmann, J., Vicedo-Cabrera, A. M., Sandstad, M., & Aunan, K. (2021). Heat stress indicators in CMIP6: Estimating future trends and exceedances of impact-relevant thresholds. *Earth's Future*, *9*(3), e2020EF001885. https://doi.org/10.1029/2020EF001885

Sherwood, S. C. (2018). How important is humidity in heat stress? *Journal of Geophysical Research: Atmospheres*, *123*(21), 11808–11810. https://doi.org/10.1029/2018JD028969

Sogacheva, L., Rodriguez, E., Kolmonen, P., Virtanen, T. H., Saponaro, G., de Leeuw, G., et al. (2018). Spatial and seasonal variations of aerosols over China from two decades of multi-satellite observations – Part 2: AOD time series for 1995–2017 combined from ATSR ADV and MODIS C6.1 and AOD tendency estimations. *Atmospheric Chemistry and Physics*, *18*(22), 16631–16652. https://doi.org/10.5194/acp-18-16631-2018

Steadman, R. G. (1984). A universal scale of apparent temperature. *Journal of Climate and Applied Meteorology*, *23*(12), 1674–1687. https://doi.org/10.1175/1520-0450(1984)023<1674:AUSOAT>2.0.CO;2

Stull, R. (2011). Wet-bulb temperature from relative humidity and air temperature. *Journal of Applied Meteorology and Climatology*, *50*(11), 2267–2269. https://doi.org/10.1175/JAMC-D-11-0143.1

Sun, X., Ren, G., Ren, Y., Liu, Y., Xue, X., & Zhang, P. (2017). A remarkable climate warming hiatus over Northeast China since 1998. *Theoretical and Applied Climatology*, *133*(1–2), 579–594. https://doi.org/10.1007/s00704-017-2205-7

Sun, Y., Zhang, X., Ren, G., Zwiers, F. W., & Hu, T. (2016). Contribution of urbanization to warming in China. *Nature Climate Change*, *6*(7), 706–709. https://doi.org/10.1038/nclimate2956

Sun, Y., Zhang, X., Zwiers, F. W., Song, L., Wan, H., Hu, T., et al. (2014). Rapid increase in the risk of extreme summer heat in Eastern China. *Nature Climate Change*, *4*(12), 1082–1085. https://doi.org/10.1038/nclimate2410

Tysa, S. K., Ren, G., Qin, Y., Zhang, P., Ren, Y., Jia, W., & Wen, K. (2019). Urbanization effect in regional temperature series based on a remote sensing classification scheme of stations. *Journal of Geophysical Research: Atmospheres*, *124*(20), 10646–10661. https://doi.org/10.1029/2019JD030948

Wang, D.-Q., & Sun, Y. (2022). Effects of anthropogenic forcing and atmospheric circulation on the record-breaking welt bulb heat event over southern China in September 2021. *Advances in Climate Change Research*, *13*(6), 778–786. https://doi.org/10.1016/j.accre.2022.11.007

Wang, F., Zheng, B., Zhang, J., Zhou, Y., & Jia, M. (2022a). Potential heat-risk avoidance from nationally determined emission reductions targets in the future. *Environmental Research Letters*, *17*(5), 055007. https://doi.org/10.1088/1748-9326/ac66f4

Wang, P., Tong, X., Qiu, J., Chen, Y., Wu, S., Chan, T. O., et al. (2022b). Amplification effect of urbanization on atmospheric aridity over China under past global warming. *Earth's Future*, *10*(5), e2021EF002335. https://doi.org/10.1029/2021EF002335

Wang, P., Yang, Y., Tang, J., Leung, L. R., & Liao, H. (2021). Intensified humid heat events under global warming. *Geophysical Research Letters*, *48*(2), e2020GL091462. https://doi.org/10.1029/2020GL091462

Wang, X., & Gong, Y. (2010). The impact of an urban dry island on the summer heat wave and sultry weather in Beijing City. *Chinese Science Bulletin*, *55*(16), 1657–1661. https://doi.org/10.1007/s11434-010-3088-5

Wang, Y., Chen, L., Song, Z., Huang, Z., Ge, E., Lin, L., & Luo, M. (2019). Human-perceived temperature changes over South China: Long-term trends and urbanization effects. *Atmospheric Research*, *215*, 116–127. https://doi.org/10.1016/j.atmosres.2018.09.006

Wu, J., Gao, X., Giorgi, F., & Chen, D. (2017). Changes of effective temperature and cold/hot days in late decades over China based on a high resolution gridded observation dataset. *International Journal of Climatology*, *37*(S1), 788–800. https://doi.org/10.1002/joc.5038

Xu, Y., Gao, X., Shi, Y., & Botao, Z. (2015). Detection and attribution analysis of annual mean temperature changes in China. *Climate Research*, *63*(1), 61–71. https://doi.org/10.3354/cr01283

Yang, Q., Li, M., Zu, Z., & Ma, Z. (2021). Has the stilling of the surface wind speed ended in China? *Science China Earth Sciences*, *64*(7), 1036–1049. https://doi.org/10.1007/s11430-020-9738-4

Yin, H., & Sun, Y. (2023). Anthropogenic influence on temperature change in China over the period 1901–2018. *Journal of Climate*, *36*(7), 2131–2146. https://doi.org/10.1175/JCLI-D-22-0122.1

Yin, H., Sun, Y., Wan, H., Zhang, X., & Lu, C. (2017). Detection of anthropogenic influence on the intensity of extreme temperatures in China. *International Journal of Climatology*, *37*(3), 1229–1237. https://doi.org/10.1002/joc.4771

Zhang, H., Luo, M., Pei, T., Liu, X., Wang, L., Zhang, W., et al. (2023a). Unequal urban heat burdens impede climate justice and equity goals. *The Innovation*, *4*(5), 100488. https://doi.org/10.1016/j.xinn.2023.100488

Zhang, J., Ren, G., & You, Q. (2023c). Supporting data for "Detection and attribution of human-perceived warming over China" [Dataset]. Zenodo. https://zenodo.org/record/10223710

Zhang, J., You, Q., Ren, G., & Ullah, S. (2022a). Projected changes in mild weather frequency over China under a warmer climate. *Environmental Research Letters*, *17*(11), 114042. https://doi.org/10.1088/1748-9326/ac9c70

Zhang, J., You, Q., Ren, G., & Ullah, S. (2023b). Substantial increase in human-perceived heatwaves in eastern China in a warmer future. *Atmospheric Research*, *283*, 106554. https://doi.org/10.1016/j.atmosres.2022.106554

Zhang, J.-T., Ren, G.-Y., & You, Q.-L. (2022b). Detection and projection of climatic comfort changes in China mainland in a warming world. *Advances in Climate Change Research*, *13*(4), 507–516. https://doi.org/10.1016/j.accre.2022.04.008

Zhang, P., Ren, G., Qin, Y., Zhai, Y., Zhai, T., Tysa, S. K., et al. (2021). Urbanization effects on estimates of global trends in mean and extreme air temperature. *Journal of Climate*, *34*(5), 1923–1945. https://doi.org/10.1175/JCLI-D-20-0389.1

Zhang, P., Ren, G., Xu, Y., Wang, X. L., Qin, Y., Sun, X., & Ren, Y. (2019). Observed changes in extreme temperature over the global land based on a newly developed station daily dataset. *Journal of Climate*, *32*(24), 8489–8509. https://doi.org/10.1175/JCLI-D-18-0733.1

Zhou, T., & Zhang, W. (2021). Anthropogenic warming of Tibetan Plateau and constrained future projection. *Environmental Research Letters*, *16*(4), 044039. https://doi.org/10.1088/1748-9326/abede8

Zhu, Y., Cao, L., Tang, G., & Zhou, Z. (2015). Homogenization of surface relative humidity over China. *Climate Change Research*, *11*(6), 379–386. https://doi.org/10.3969/j.issn.1673-1719.2015.06.001